Observation of a high-temperature incommensurate phase transition and discommensurations in $TaTe_4$

1991 J. Phys.: Condens. Matter 3 6959

(http://iopscience.iop.org/0953-8984/3/36/001)

J. Phys.: Condens. Matter 3 (1991) 6959–6972. Printed in the UK

Observation of a high-temperature incommensurate phase transition and discommensurations in $TaTe_4$

J C Bennett†, F W Boswell†, A Prodan‡, J M Corbett† and S Ritchie†

† Guelph-Waterloo Program for Graduate Work in Physics, Waterloo Campus, Waterloo, Ontario, Canada N2L 3G1

‡ Institut J Stefan, Jamova 39, 61000 Ljubljana, Slovenia

Received 15 April 1991, in final form 4 June 1991

Abstract. The tetrachalcogenides $TaTe_4$ and $NbTe_4$ provide an excellent model system for the study of charge-density wave (CDW) phenomena in quasi-one-dimensional materials. $TaTe_4$ is commensurately modulated at room-temperature and, upon heating, has been observed to undergo a commensurate-to-commensurate phase transition at about 450 K. In this paper, we report an additional commensurate-to-incommensurate transition occurring above 550 K. Satellite dark-field electron microscopy reveals the presence of defects in the microstructure of the high-temperature phases including discommensuration arrays in the incommensurate state. The evolution of the discommensuration arrays during heating and cooling through the 550 K transition is reported. These results are discussed in relation to the sequence of phase transitions previously observed for the isostructural incommensurate compound $NbTe_4$ on cooling below room-temperature.

1. Introduction

Over the past several years, experimental and theoretical investigations of the tetrachalcogenides $TaTe_4$ and $NbTe_4$ by a number of researchers have demonstrated that these compounds constitute a prototypical system for the study of charge-density wave (CDW) modulations. The compounds have a quasi-one-dimensional crystal structure in which chains of metal atoms are centred within extended cages of Te atoms in square antiprismatic coordination. The observed lattice distortions, involving mainly longitudinal motions of metal atoms along a chain, correspond to that of the classic CDW model. In addition, the compounds exhibit the full spectrum of possible CDW-driven phase transitions: commensurate-to-incommensurate (C to IC), commensurate-to-commensurate (C to C) and incommensurate-to-incommensurate (IC to IC).

The subcell structures of $TaTe_4$ [1] and $NbTe_4$ [2] were first reported in the early 1960s as being based on a tetragonal unit cell (figure 1) with axes ($a \times a \times c$). Relatively little attention was paid to these compounds, however, until Boswell *et al* [3] reported the presence at room-temperature of a ($2a \times 2a \times 3c$) commensurate superstructure for $TaTe_4$ and a ($\sqrt{2}a \times \sqrt{2}a \times \sim 16c$) incommensurate modulation structure for $NbTe_4$. Several subsequent studies confirmed these results [4, 5]. A detailed structural analysis by Bronsema *et al* [6] and a high-resolution electron microscopy study by Corbett *et al* [7] established the space group of the room-temperature commensurate phase of $TaTe_4$ as $P4/ncc$, in agreement with the Landau theory study of Walker [8]. Using a superspace

0953-8984/91/366959 + 14 $03.50

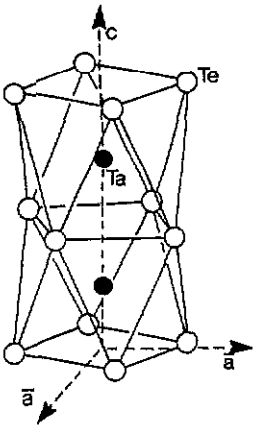

Figure 1. The tetragonal subcell structure of $TaTe_4$ and $NbTe_4$. Full circles represent metal atoms and open circles Te atoms.

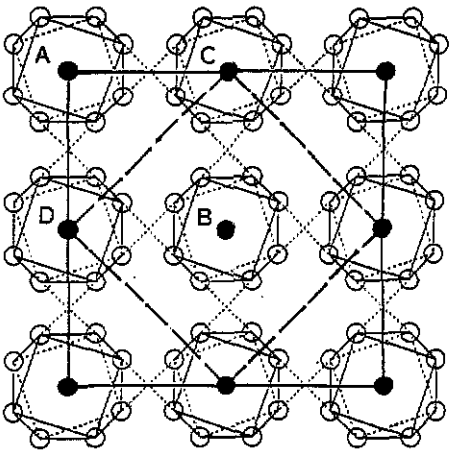

Figure 2. Schematic representation of the room-temperature modulation structures of $TaTe_4$ and $NbTe_4$ projected along the c-axis. For $TaTe_4$, the CDW phasings along the columns are $\varphi_A = 2\pi/3$, $\varphi_B = 4\pi/3$ and $\varphi_C = \varphi_D = 0$ generating a unit cell of basal plane dimension $2a \times 2a$ (solid line). For $NbTe_4$, the column phasings are $\varphi_A = \varphi_B = \pi$ and $\varphi_C = \varphi_D = 0$ resulting in basal plane unit cell dimensions of $\sqrt{2}a \times \sqrt{2}a$ (dashed line).

group description [9], the room-temperature modulation structure of $NbTe_4$ was found to belong to $W^{P4_2mc}_{11\,11}$ by van Smaalen *et al* [10], again in agreement with the predictions of Walker [8]. A schematic representation of the room-temperature modulation structures of $TaTe_4$ and $NbTe_4$ is shown in figure 2. Several studies have also revealed that a complete range of solids solutions exists for $Ta_{1-x}Nb_xTe_4$ ($0 \leq x \leq 1$) and several new incommensurate phases are stabilized at room-temperature [11, 12].

In addition to the room-temperature structures, several other modulated phases become stable in the $TaTe_4/NbTe_4$ system upon heating or cooling. These new phases, and also the nature of the transitions between them, have been observed by electron diffraction and electron microscopy *in situ*. A high-temperature transition to a $(\sqrt{2}a \times \sqrt{2}a \times 3c)$ commensurate phase has been reported by Boswell *et al* [13] to occur in $TaTe_4$ on heating above 450 K. $NbTe_4$ exhibits a lock-in phase transition around 50 K to a $(2a \times 2a \times 3c)$ unit cell which is apparently isostructural with room-temperature $TaTe_4$ [3, 4, 14, 15]. In addition, electron diffraction experiments have revealed that elongated streaks parallel to c^* have developed into sharp, closely spaced satellite spots upon cooling $NbTe_4$ below about 200 K [16]. The origin of these additional satellites has been attributed to the presence of a new incommensurate phase with base $(2a \times 2a)$ existing in the temperature range 50 to 200 K [15, 17]. Several theoretical papers [18, 19] have appeared which deal with the IC to IC phase transition in $NbTe_4$. Walker and Morelli [18] have proposed a model in which discommensurations ('walls' between commensurate domains) are optimally phased in adjacent columns in order to minimize the overall free energy of the crystal. In this model, the temperature dependant driving mechanism of the phase transition involves a competition between first-neighbour and second-neighbour column interactions [19].

Domain boundaries in the room-temperature modulated structure of $TaTe_4$ were first observed by Eaglesham *et al* [14] using satellite dark-field (SDF) electron microscopy. Boswell *et al* [13] concluded the domain boundaries result from phasing errors of the CDW on adjacent columns associated with rapid cooling through the high-temperature C to C phase transition at 450 K. Discommensuration arrays in $NbTe_4$ and their behaviour as a function of temperature have also been reported [4, 14, 15]. SDF images show that the discommensuration arrays are replaced during an extremely sluggish lock-in transition at 50 K by a network of commensurate domains reminiscent of those observed in room-temperature $TaTe_4$.

In this paper, we report a new incommensurate phase of $TaTe_4$ above 550 K. SDF microscopy has been used to reveal that the transition is mediated by the formation of discommensurations. These observations provide additional insight into the complex processes which stabilize the various phases and further illustrate the rich diversity of phenomena occurring in this 'simple' system.

2. Experimental details

The crystals were grown from the elements in evacuated quartz tubes, using iodine as a transport agent, as described elsewhere [3]. The tubes were heated at 800 °C for several days, slowly cooled to 600 °C, held at this temperature for 20 h and then quenched to room temperature. The crystals generally grew in the form of bundles of parallel needles. Specimens for electron microscopy were obtained by cleaving these needles between the glass slides. This results in a large number of small crystallites with electron transparent edges parallel to the chain axis. The specimens were examined at 100 kV using a Philips EM300 electron microscope equipped with a single-tilt heating stage.

3. Results

3.1. Electron diffraction

Electron diffraction patterns (EDPs) of $TaTe_4$ at elevated temperatures indicate the occurrence of two distinct structural phase transitions: a C to C transition at approximately 450 K and a C to IC transition near 550 K. At room temperature, the superlattice spots appear in commensurate positions and may be completely indexed using the three modulation wave-vectors $\boldsymbol{q}_1 = [\frac{1}{2}\boldsymbol{a}^*, \frac{1}{2}\boldsymbol{b}^*, \frac{2}{3}\boldsymbol{c}^*]$, $\boldsymbol{q}_2 = [\frac{1}{2}\boldsymbol{a}^*, 0, \frac{2}{3}\boldsymbol{c}^*]$ and $\boldsymbol{q}_3 = [0, \frac{1}{2}\boldsymbol{b}^*, \frac{2}{3}\boldsymbol{c}^*]$ defined relative to the subcell. When heated above 450 K, the satellites associated with wave-vectors $\boldsymbol{q}_2$ and $\boldsymbol{q}_3$ diminish in intensity and gradually disappear over a narrow temperature range (~30 K) while those associated with $\boldsymbol{q}_1$ remain unchanged. The phase transition is reversible with the $\boldsymbol{q}_2$ and $\boldsymbol{q}_3$ satellite reflections reappearing if the temperature is slightly lowered. These observations can be interpreted in terms of a transformation to a high-temperature commensurately modulated phase with unit cell $(\sqrt{2}a \times \sqrt{2}a \times 3c)$ as discussed previously by Boswell *et al* [13].

Further changes occurred in the EDPs of $TaTe_4$ upon heating above approximately 550 K. The remaining superlattice satellites shift to incommensurate positions defined by the modulation wave-vector $\boldsymbol{q}_1 = [\frac{1}{2}\boldsymbol{a}^*, \frac{1}{2}\boldsymbol{b}^*, 0.6630 \pm 0.0010\boldsymbol{c}^*)$. Although the deviation from the commensurate value is only ~0.6%, the incommensurate nature of the modulation is clearly revealed in [130] zone axis EDPs (figure 3) by the presence of satellite

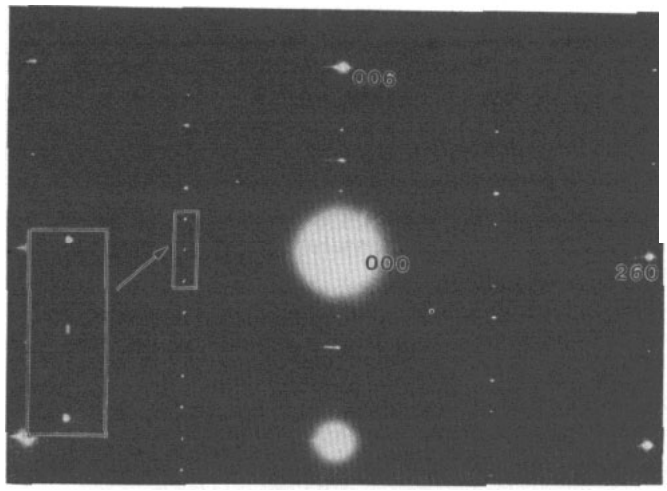

Figure 3. [130] zone axis electron diffraction pattern from $TaTe_4$ at 550 K; the superlattice doublet revealing the incommensurate periodicity is enlarged in the inset.

doublets centred about the commensurate positions. Note that the change in the modulation periodicity is in the opposite sense to that observed for incommensurate $NbTe_4$, i.e. the c^*-component of the q-vector is reduced below the commensurate value rather than increased. No further change in the q-vector has yet been observed on heating above 550 K, however, the proximity of the transition to the decomposition point greatly restricts the available temperature range as discussed below. We propose that the electron diffraction observations are the result of the development of an incommensurate phase of $TaTe_4$ above 550 K having basal plane dimensions ($\sqrt{2}a \times \sqrt{2}a$). The phase transition is reversible but exhibits considerable temperature hysteresis, occurring near 450 K on cooling.

Although the C to IC phase transition occurs very near the temperature at which $TaTe_4$ will decompose under the conditions prevailing in the electron microscope, it is normally possible to cycle a crystal through the phase transition several times without any indication of decomposition. It is, however, difficult to control the specimen temperature precisely using the heating holder in the electron microscope since observations are usually made on a small, thin region of a larger crystal whose thermal contact with the support grid may vary during the experiment. As a result, an unambiguous determination of whether the C to IC transition is discontinuous or continuous in a narrow temperature range has not been possible. Also, these experimental difficulties may explain why the C to IC transition was not observed by previous workers [3, 15].

3.2. Satellite dark-field microscopy

3.2.1. The commensurate-to-commensurate phase transition. SDF images of $TaTe_4$ obtained at room temperature typically reveal a three-dimensional network of antiphase boundaries (APBS). From the diffraction contrast, two main types of APBS can be distinguished: type I boundaries generally lying along the c-axis direction with an associated displacement vector of the form $\boldsymbol{R}_1 = \frac{1}{2}\{110\}$ and type II boundaries which lie inclined to the c-axis in an irregular manner with displacement vectors of the from $\boldsymbol{R}_2 = \frac{1}{6}\{302\}$

[13]. The type II boundaries exhibit contrast for all satellite reflections while the type I boundaries are out of contrast in SDF images formed using the q_1 satellites (figure 4 (*a*), (*a'*)). Type I boundaries are frequently observed to terminate at a junction with two type II boundaries.

The behaviour of the APBs upon heating to the C to C transition at 450 K has been observed by SDF microscopy. In SDF images formed using a q_2 or q_3 satellite, all of the APBs exhibit dark contrast (at $s = 0$) and were fairly narrow at room temperature. When the specimen was heated, some movement of the type II boundaries usually occurred sightly below the transition temperature. The motion of the type II boundaries resulted in progressively shorter type I boundaries as the temperature was increased until, very near the transition, the type I boundaries were almost entirely eliminated. The disappearance of the type I boundaries as accompanied by a noticeable increase in the width of the remaining type II boundaries. Very near the transition temperature, the boundaries were unstable and often expanded to convert an appreciable region of the specimen to dark contrast, i.e. a region of the high-temperature commensurate phase. On further heating, essentially the entire specimen is converted to dark contrast. This coincides with the disappearance of the q_2 and q_3 satellites in the EDPs. The above effects are shown in figures 4(*b*), (*c*), (*d*). Based on the SDF images, it appears the phase transition is initiated at the APBs and spreads outward through the crystal. It should be noted, however, that the regions of elevated temperature commensurate phase do not form symmetrically but instead exhibit a definite tendency to expand outward from only one side of a given domain boundary. All of the observed phenomena were reversible with temperature. Similar effects are observed in SDF images formed using the q_1 satellites (figures 4(*b'*), (*c'*), (*d'*)).

When a specimen is heated above the C to C transition temperature, SDF images obtained using q_2 or q_3 satellites show essentially dark contrast throughout the field of view. In all of the crystals studied, however, a few narrow regions exhibiting faint light contrast are visible (figure 4(*d*)). The area of light contrast are observed along the line of intersection between two expanding regions of dark contrast and, since the areas of dark contrast usually spread out in only one direction, are most often observed near the positions of the type II boundaries in the room-temperature phase. SDF images formed using q_1 satellites clearly reveal these as domain boundaries in the high-temperature commensurate phase (figure 4(*d'*)). From the geometrical relationship between these high-temperature APBs and the type II boundaries found in the room-temperature structure, we propose that the displacement vectors are identical, i.e. $\boldsymbol{R} = \frac{1}{6}[302]$ or $\frac{1}{6}[032]$ which, indexed in terms of the high-temperature $\sqrt{2}a \times \sqrt{2}a \times 3c$ unit cell, are equivalent to $\boldsymbol{R} = \frac{1}{6}[332]$.

3.2.2. The commensurate-to-incommensurate phase transition. The microstructure of the high-temperature commensurate phase continues to evolve as the crystal is heated towards the incommensurate transition. Following the 450 K transition relatively few APBs are visible in SDF images formed with the q_1 satellites (figure 4(*d'*)). As the temperature is increased above 450 K, the defects gradually evolve into multiple lines and expand to cover large regions of the crystal (figure 5(*a*)). The defect density continues to increase with temperature until eventually, near 550 K, a regular array of 'fringes' with a separation of ~200 Å is observed (figure (5*b*)). Selected-area EDPs reveal the crystal is incommensurate in this fringe state. In analogy with the model of the discommensurate state proposed for $NbTe_4$ by Mahy *et al* [15], the fringes are interpreted as arising from the generation of discommensuration walls perpendicular to the fibre

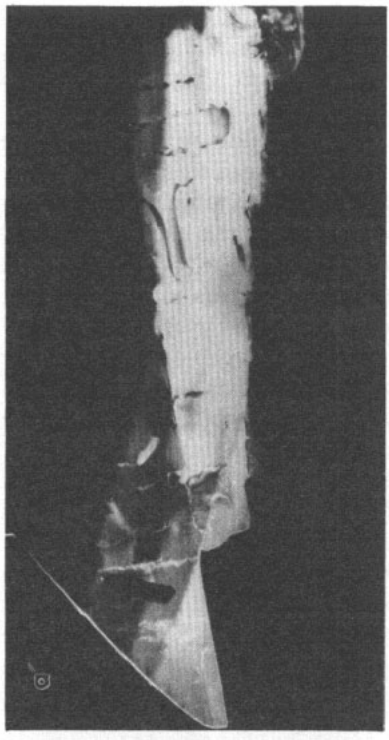

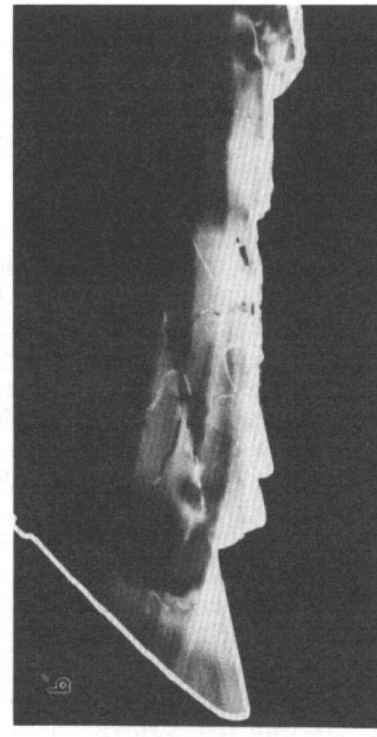

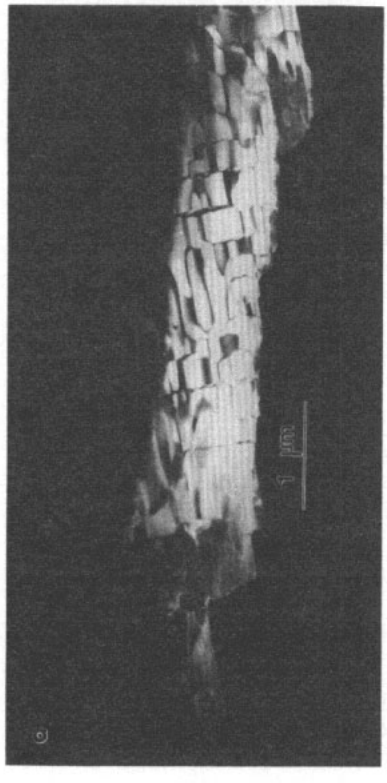
1 mm

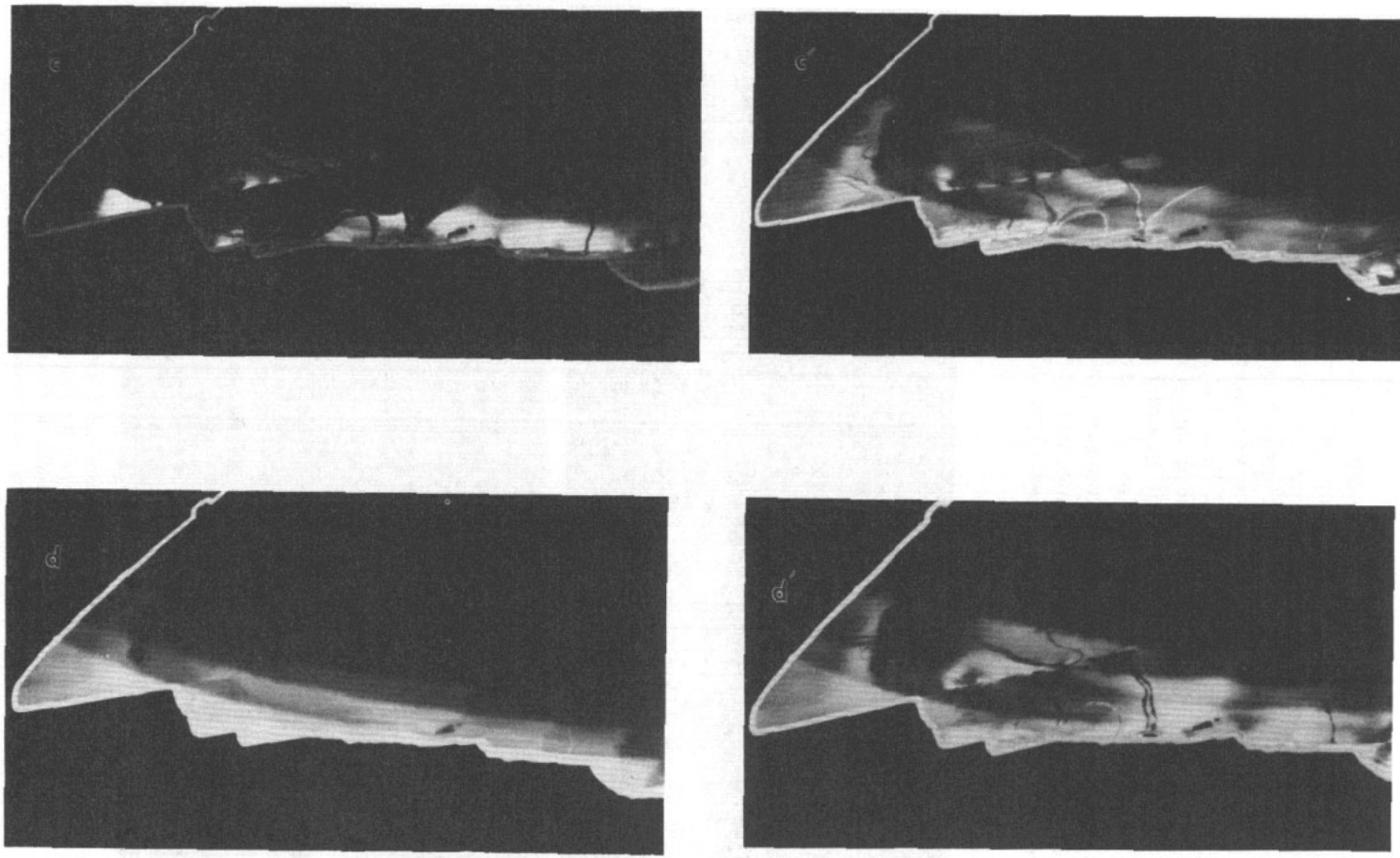

Figure 4. (018) and (028)—indicated by prime—SDF images of the same region of $TaTe_4$ crystal observed during heating to the commensurate-to-commensurate transition temperature $T_C \sim 450$ K. *(a, a') at room-temperature, (b, b') heated to nearly T_C, (c, c') heated to T_C and (d, d') heated to slightly above T_C.*

axis (note here a discommensuration wall is defined as the set of all one-dimensional discommensurations projected in a given plane normal to the *c*-axis). The somewhat variable spacing of the fringes is apparently a consequence of disorder in the discommensuration array. On heating, the mechanism for increasing the discommensuration wall density appears to involve the internal nucleation and motion of 'discommensuration-dislocations', each consisting of a six-fold junction of discommensuration walls. An example of this is shown in figure 5(*a*). Similar phenomena have been observed in $NbTe_4$ as well as for 2H-$TaSe_2$ [20], Rb_2ZnCl_4 [21] and certain Ag–Mg alloys [22], all of which undergo a C to IC phase transition. Since the phase transitions in $TaTe_4$ take place extremely rapidly (of the order of seconds) over a narrow temperature range, it has not been possible to follow the discommensuration process in detail. It does appear, however, that discommensuration walls in some cases can also be formed without the action of discommensuration-dislocations. The mechanism, suggested by Walker and Morelli [18], in which the discommensuration walls separate

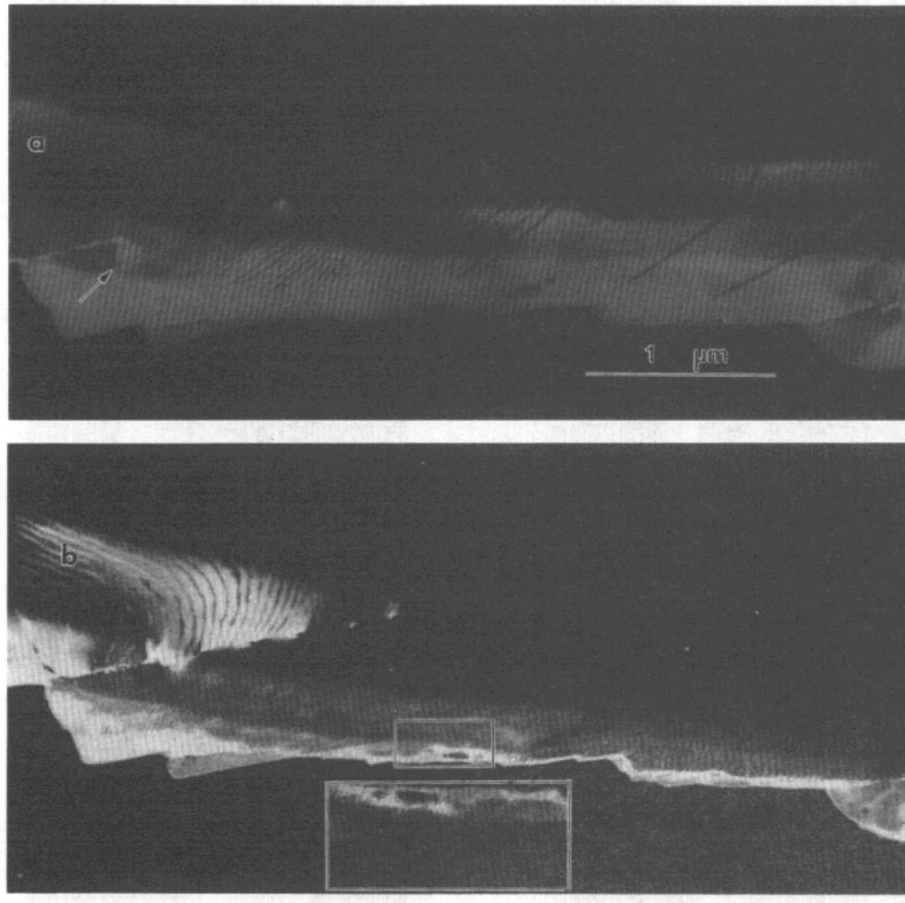

Figure 5. (028) SDF images of the same region of a $TaTe_4$ crystal observed during heating to the commensurate-to-incommensurate transition $T_{IC} \sim 550$ K. The crystal has been heated slightly between (*a*) and (*b*). A six-fold junction of defects is indicated by an arrow in (*a*). The inset in (*b*) shows the marked region at higher magnification.

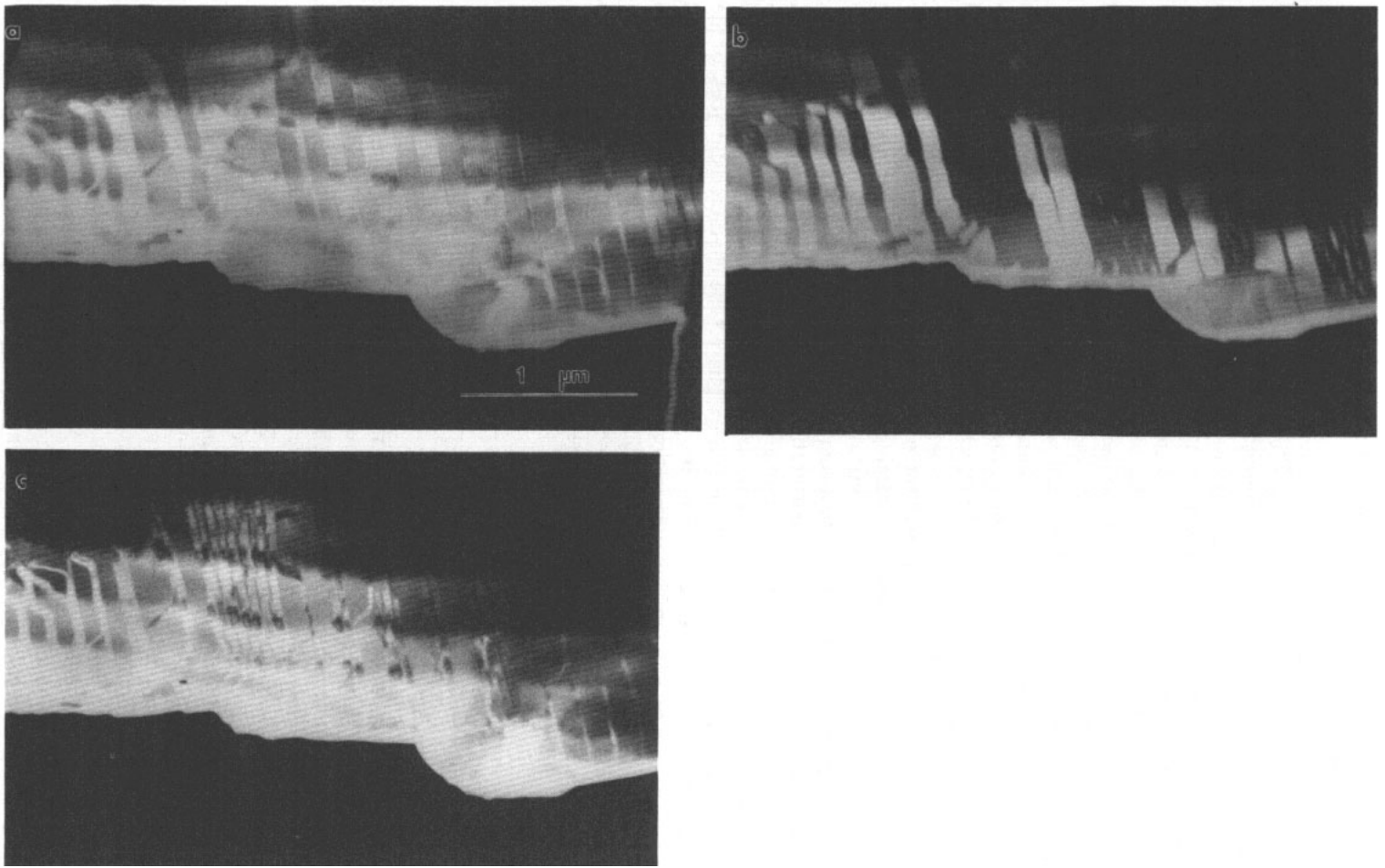

Figure 6. (*a*) ( )28) and (*b*) (018) SDF images of $TaTe_4$ duri g l ck-in. The temp rature of the crystal has decreased by a few degrees betwe n (*a*) and (*c*)

to form pairs in response to temperature dependent variations in the free energy may also play a role in the process.

Once established, the discommensurate state of $TaTe_4$ persists on cooling to near 450 K, the transition temperature of the $(2a \times 2a \times 3c)$ commensurate phase. Unlike $NbTe_4$, a precursor stage in which the crystal adopts a structure with $2a$ basal plane dimensions is apparently not required for lock-in. This is shown in SDF images formed with q_1 satellites which exhibit dark bands running perpendicular to the c-axis (figure 6(a)) coexisting with well-defined bands of parallel discommensuration walls. The dark bands exhibit bright contrast when imaged using a q_2 or q_3 satellite, indicating these are regions of the room-temperature commensurate phase (figure 6(b)). These dark bands are, in fact, rarely continuous across the width of the crystal but are instead typically segmented by discommensuration walls running roughly parallel to the c-axis. Additional patches of commensurate material nucleate and expand to form bands on further cooling. Eventually, at a temperature slightly below the C to C transition, the commensurate bands cover the entire crystal with the exception of a relatively small number of faults, principally the type II APBs identified previously.

The SDF observations indicate that the mechanisms involved in increasing the discommensuration wall density during heating are different from those which occur on cooling the crystals through the high-temperature phase transitions. This may help to explain the marked thermal hysteresis associated with the transitions in both the $TaTe_4$ and $NbTe_4$. On cooling, the discommensuration array is fragmented by the development of the commensurate bands, typically into groupings of three discommensuration walls (figure 6(c)). On further cooling, these triplets of defects appear to coalesce along their length leaving an APB in the room-temperature phase. The characteristic 'jogs' of the discommensuration walls appear to limit the growth of the commensurate domains and represent an energetically stable configuration. We suggest that these jogs are precursors to the type I APBs observed in the room-temperature phase, the reduction in the discommensuration wall density then being mediated by the formation and motion of a junction of a type I boundary with two type II boundaries.

4. Discussion

4.1. The CDW phases of $NbTe_4$ and $TaTe_4$

An extensive number of experimental and theoretical studies have culminated in the emergency of a fairly clear picture of the CDW states of $NbTe_4$ [5, 6, 10, 11, 15, 17–19]. The incommensurate phase having a unit cell $(\sqrt{2}a \times \sqrt{2}a \times \sim 16c)$ is stable at room-temperature. A transition to a new incommensurate ('discommensurate') phase or phases occurs in the temperature range 50–200 K, albeit with a considerable thermal hysteresis between cooling and warming cycles. Prodan *et al* [17] have proposed the coexistence of two incommensurate phases in this temperature range: a phase denoted LT_1, with unit cell $(2a \times 2a \times \sim 16c)$ involving mainly longitudinal shifts of the atoms from their room-temperature positions and a second phase denoted LT_2 with a unit cell $(2a \times 2a \sim 32c)$ which is associated with transverse displacements of the Te atoms. Below 50 K, a $(2a \times 2a \times 3c)$ commensurate phase is stable.

$TaTe_4$, on the other hand, has a $(2a \times 2a \times 3c)$ commensurate superstructure at room-temperature which is apparently isostructural with the lock-in phase of $NbTe_4$, although this has yet to be verified by low-temperature x-ray analysis. On heating $TaTe_4$

to approximately 450 K, a transition to a ($\sqrt{2}a \times \sqrt{2}a \times 3c$) commensurate phase occurs. This transition is strongly first-order, as is the lock-in transition in $NbTe_4$. However, unlike the sluggish process in that compound, the transition in $TaTe_4$ takes place rapidly within a narrow temperature range of approximately 10 K. The c^*-component of the modulation wave-vector adopts an incommensurate value on heating above 550 K. On cooling from the high-temperature incommensurate state, lock-in to a commensurate state does not occur for $TaTe_4$ until about 450 K. This is similar to the behaviour observed for $NbTe_4$ where the commensurate phase persists to a much higher temperature on warming (~150 K) than on cooling (~50 K).

It has been shown in the series of papers by Walker and coworkers [8, 18, 19, 23, 24, 25] that the phase transitions in $NbTe_4$, which result in a change in the basal plane dimensions, are driven primarily by subtle variations in the intercolumn interaction strengths occurring as a function of temperature. It is the intercolumn interactions that dictate the relative phasing of the CDW on the otherwise equivalent columns. The temperature dependences of the first- and second-neighbour column interactions are such that antiphased CDW are favoured at room-temperature while, at lower temperatures, a $2\pi/3$ phase shift between columns is preferred. The basal plane dimensions are correspondingly enlarged from $\sqrt{2}a$ to $2a$. We note that the form of the LT_1 distortion [17] agrees with the model of the low-temperature incommensurate state proposed by Morelli and Walker [19] from a consideration of the intercolumn energetics. The displacements associated with the LT_2 phase, which result in a distortion of the Te cages, are also consistent with a mechanism driven by intercolumn interactions, although this distortion mode appears to be outside the scope of the theoretical analyses of Walker and coworkers where only Nb displacements were considered. In terms of the crystal structure, the important role of intercolumn forces is reflected in the maintenance of near constant intercolumn Te–Te bond lengths in all of the modulated phases [10, 26].

As for the low-temperature IC to IC transition observed in $NbTe_4$, the C to C phase transition in $TaTe_4$ also involves a change in the basal plane dimensions from $2a$ to $\sqrt{2}a$. Chen *et al* [24] have proposed that the transition occurs as a consequence of a change in the sign of the third-neighbour column interaction energy and predict $P4/ncc$ symmetry for the high-temperature commensurate phase. In this model, the CDW modulations are out of phase on adjacent columns and in phase on second neighbour columns. With reference to figure 2, the CDW phases on the respective columns are $\varphi_A = \varphi_B = \theta$ and $\varphi_C = \varphi_D = -(\theta + 2\pi/3)$ where θ is an arbitrary angle. Note that this is in contrast to $NbTe_4$ where the symmetry of the room-temperature phase with base $\sqrt{2}a$ is $P4/mcc$ and the CDW on adjacent columns are antiphased. An alternative model for high-temperature commensurate $TaTe_4$ with symmetry $P4/mcc$ and CDW phasing $\varphi_{A,B} = \varphi_{C,D} + \pi$ has also been proposed [27]. In this case, the phasing is similar to that observed for room-temperature $NbTe_4$. An experimental determination of the symmetry to resolve this question is not yet available.

For both the $P4/ncc$ and $P4/mcc$ models described above, two energetically equivalent columns constitute the high-temperature unit cell. Since all three columns in the room-temperature phase are also equivalent, any two of these may be used to form the high-temperature structure. As a result, several different energetically equivalent configurations of the high-temperature cell are possible (figure 7). The rapid completion of the C to C transition in $TaTe_4$ suggests a minimal rearrangement of the CDW phasings occurs. The model of the high-temperature state possessing $P4/ncc$ symmetry appears to be more consistent with this requirement.

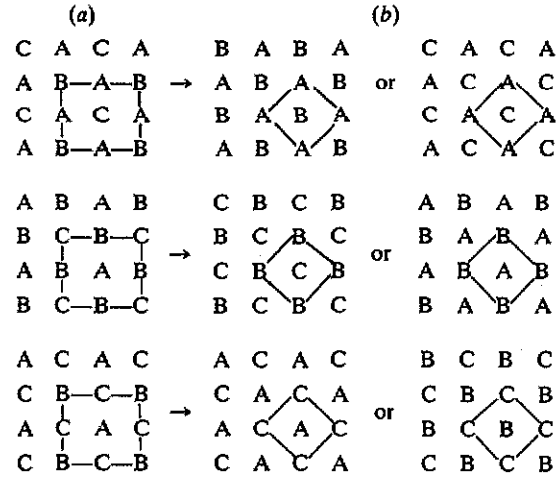

Figure 7. Proposed model for the high-temperature modulation structure of $TaTe_4$ viewed along the *c*-axis. The different possible unit cell configurations of these columns in the (*a*) room-temperature and (*b*) high-temperature structures are sketched.

4.2. Origin of the defects in the high-temperature commensurate phase of $TaTe_4$

The origin of the defects observed by SDF microscopy in the high-temperature commensurate phase may be explained as follows. At the transition, regions of elevated temperature phase nucleate at faults in the room-temperature structure and, with a further increase in temperature, expand throughout the crystal. If, during this process, two regions composed of different configurations of the high-temperature unit cell expand into each other, an APB will be formed along the line of intersection. The displacement vector associated with these APBs in the high-temperature structure is of the form $\boldsymbol{R} = \frac{1}{8}$ [332]. Nucleation of different configurations of the high-temperature structure will be favoured on opposite sides of a room-temperature APB, possibly accounting for the observed expansion of the APBs in only one direction on heating. Conversely, on cooling, the nucleation of the room-temperature structure is promoted at the APBs of the high-temperature phase since, as required, nearest-neighbour columns are already shifted in phase by $2\pi/3$ while the second-neighbour columns are in phase in these regions.

4.3. Discommensurations in $TaTe_4$

SDF microscopy indicates that discommensurations play a significant role in the incommensurate phases of both $TaTe_4$ and $NbTe_4$. The deviation of the CDW period from a commensurate value leads to the generation of one-dimensional discommensurations along the columns, i.e. metal atom multiplets of a different nature than the predominant triplet sequence. In the case of $NbTe_4$, the structural refinement of Van Smaalen *et al* [10] shows that discommensurations appear along the chains with a periodicity of 16*c* and consist of an approximate doublet-singlet-doublet-singlet-doublet sequence. The 'discommensuration' thus has a considerable extent and, since the structure was derived based on a sinusoidal modulating function, the associated phase slip is gradual than abrupt. The calculations of Prodan *et al* [17] suggest this is also the case for the discommensurations present in the LT incommensurate phases. Antiphasing of the CDW on

adjacent columns results in the projected arrays of the discommensurations, i.e. the discommensuration walls, being separated by 8*c* as discussed by Mahy *et al* [15]. In the incommensurate state of $TaTe_4$, regular arrays of discommensuration walls are also observed in SDF images with an equilibrium spacing of about 200 Å (~27*c*). These discommensurations are also likely to involve a gradual rather than abrupt phase slip. Thus, in both $NbTe_4$ and $TaTe_4$, the incommensurate states are discommensurate in character. Similarly, in both compounds, the discommensuration arrays evolve on heating from faults in the commensurate structures. However, the basal dimensions of the supercells in which these faults appear differ for $NbTe_4$ and $TaTe_4$ being 2*a* and $\sqrt{2}a$ respectively. As a result, the mechanism proposed by Mahy *et al* for the generation of discommensuration arrays in $NbTe_4$, which involves elements of the 2*a* to $\sqrt{2}a$ transformation, does not appear to be strictly applicable to the $TaTe_4$ case.

In $TaTe_4$, the faults in the high-temperature commensurate phase gradually become more numerous and regularly spaced as the temperature is increased until, ultimately a uniform array is formed in the incommensurate state. While the study of the evolution of the discommensuration arrays has been restricted by the inherent instabilities of the heating stage which limit resolution to about 100 Å, the SDF images suggest that the C to IC transition observed on heating may be continuous. Note that Morelli and Walker [19] have proposed the IC to IC transition in $NbTe_4$ could be continuous if a repulsive interaction exists between the discommensuration walls. An experimental determination regarding this point has not been possible with the single-tilt heating holder used in these studies. It is usually necessary to tilt the specimen away from the zone axis condition to obtain sufficient intensity in the SDF images, while zone axis EDPs are needed for accurate measurements of the *q*-vector. Thus, it has not been possible to obtain direct evidence of a possible continuous variation of the *q*-vector from the commensurate to the incommensurate state. Further studies, employing a double-tilt heating stage may resolve this question.

SDF images of $NbTe_4$ and $TaTe_4$ obtained during cooling from the incommensurate state exhibit a remarkable similarity (cf figure 5 with figure 10 of [14]). For both compounds, bands of the commensurate phase become more numerous as lock-in progresses. However, the tendency noted by Eaglesham *et al* [14] for these commensurate bands in $NbTe_4$ to drive across the incommensurate regions is not often observed for $TaTe_4$, suggesting this phenomenom may have been associated with a temperature gradient. Also, the transition in $TaTe_4$ proceeds very rapidly without the formation of precursor phases analogous to the incommensurate LT_1/LT_2 phases observed for $NbTe_4$. This implies thermal energies play an important role in the transition processes in these materials.

Overall, the results of the current study of the high-temperature phase transitions in $TaTe_4$ are broadly consistent with the picture that has emerged of the transitions occurring below room-temperature in $NbTe_4$. The differences as well as similarities in the transition processes provide new insight into the nature of the CDW modulations in these compounds.

Acknowledgments

The authors wish to acknowledge the financial support of the Natural Sciences and Engineering Research Council of Canada and the assistance of P Stillwell in growing the bulk crystals.

References

[1] Bjerkelund E and Kjekshus A 1964 *J. Less-Common Met.* **7** 231
[2] Selte K and Kjekshus A 1964 *Acta Chem. Scand.* **18** 690
[3] Boswell F W, Prodan A and Brandon J K 1983 *J. Phys. C: Solid State Phys.* **16** 1067
[4] Mahy J, van Landuyt J, Amelinckx S, Uchida Y, Bronsema K D and van Smaalen S 1985 *Phys. Rev. Lett.* **55** 11
[5] Böhm H and Von Schnering H G 1985 *Z. Kristallogr.* **171** 41
[6] Bronsema K D, van Smaalen S, de Boer J, Wiegers G A and Jellinek F 1987 *Acta Cryst.* B **43** 305
[7] Corbett J M, Hiltz L G, Boswell F W, Bennett J C and Prodan A 1988 *Ultramicroscopy* **26** 43
[8] Walker M B 1985 *Can. J. Phys.* **63** 46
[9] de Wolff P M, Jansen T and Janner A 1981 *Acta Crystallogr.* A **37** 625
[10] van Smaalen S, Bronsema K D and Mahy J 1986 *Acta Crystallogr.* B **42** 43
[11] Boswell F W and Prodan A 1984 *Mat. Res. Bull.* **19** 93
[12] Bennett J C, Boswell F W, Corbett J M, Prodan A and Kohara S 1990 *Proc. XIIth Int. Congress for Elect. Microscopy* 170
[13] Boswell F W, Prodan A, Bennett J C, Corbett J M and Hiltz L G 1987 *Phys. Status Solidi* a **102** 207
[14] Eaglesham D J, Bird D M, Withers R L and Steeds J W 1985 *J. Phys. C: Solid State Phys.* **18** 1
[15] Mahy J, van Landuyt J, Amelinckx S, Bronsema K D and van Smaalen S 1986 *J. Phys. C: Solid State Phys.* **19** 5049
[16] Boswell F W and Prodan A 1986 *Phys. Rev.* B **34** 2979
[17] Prodan A, Boswell F W, Bennett J C, Corbett J M, Vidmar T, Marinkovic V and Budkowski A 1990 *Acta Crystallogr.* B **46** 587
[18] Walker M B and Morelli R 1988 *Phys. Rev.* B **38** 4826
[19] Morelli R and Walker M B 1989 *Phys. Rev. Lett.* **62** 1520
[20] Fung K K, McKernan S, Steeds J W and Wilson J A 1981 *J. Phys. C: Solid State Phys.* **14** 5417
[21] Tsuda K, Yamamoto N and Yagi K 1988 *J. Phys. Soc. Japan* **57** 2057
[22] Fujino Y, Sato H, Hirabayashi M, Aoyagi E and Koyama Y 1987 *Phys. Rev. Lett.* **58** 1012
[23] Sahu D and Walker M B 1985 *Phys Rev.* B **32** 1643
[24] Chen Z Y and Walker M B 1989 *Phys. Rev.* B **40** 8983
[25] Chen Z Y, Walker M B and Morelli R 1989 *Phys. Rev.* B **39** 11742
[26] Kucharczyk D, Budkowski A, Boswell F W, Prodan A and Marinkovic V 1990 *Acta Crystallogr.* B **46** 587
[27] Budkowski A 1990 private communication